Title

A STUDY OF FACTORS THAT AFFECT THE PRECISION OF COMPARTMENTAL MODEL PARAMETER ESTIMATION USING DYNAMIC POSITRON EMISSION TOMOGRAPHY

Authors

Mazoyer, B.M.
Huesman, R.H.
Budinger, T.F.
et al.

Publication Date

1985-05-01

LBL-19614
Preprint

Lawrence Berkeley Laboratory
UNIVERSITY OF CALIFORNIA

Submitted to the Journal of Computer
Assisted Tomography

A STUDY OF FACTORS THAT AFFECT THE PRECISION OF COMPARTMENTAL MODEL PARAMETER ESTIMATION USING DYNAMIC POSITRON EMISSION TOMOGRAPHY

B.M. Mazoyer, R.H. Huesman, T.F. Budinger,
and B.L. Knittel

May 1985

Prepared for the U.S. Department of Energy under Contract DE-AC03-76SF00098

DISCLAIMER

A STUDY OF FACTORS THAT AFFECT THE PRECISION OF COMPARTMENTAL MODEL PARAMETER ESTIMATION USING DYNAMIC POSITRON EMISSION TOMOGRAPHY

B. M. MAZOYER, R. H. HUESMAN, T. F. BUDINGER, and B. L. KNITTEL

Donner Laboratory and Lawrence Berkeley Laboratory,
University of California, Berkeley, CA 94720

LBL - 19614

Submitted for publication

Abstract

A method for comparison and optimization of experimental designs (rate of injection and rate of tomographic data collection) of emission tomography studies is proposed. The sensitivity matrix of the study model and an estimate of the statistical uncertainty of the tomographic data are used to compute the covariance matrix of the parameters. The determinant of this covariance matrix (proportional to the total volume of uncertainty of the model parameters) serves as a criterion to be minimized. The method is applied to brain glucose metabolism studies using dynamic positron emission tomography, and a comparison of various current protocols is made with simulated data. The results show that higher rates of injection and higher rates of data collection at early times lead to smaller statistical uncertainties of the parameter estimates. Sources of biases in these estimates are also investigated; this study shows that the model must account for the integration process inherent to the tomographic data collection, as well as include the vascular fraction and the time difference between the arrival of the tracer at the blood sampling site and at the tomographic region.

Introduction

This paper presents a method for evaluation of input functions (rate of injection) and of temporal sampling strategies (rate of tomographic data collection) for emission tomography. This is the first attempt, to our knowledge, to calculate a quality factor for a given strategy and to optimize the experimental design of emission tomography studies.

The determination of physiological properties (such as tissue blood flow, metabolic rates, receptor activity, substrate turnover or clearance) relies on accurate measurements of the response of a tissue or organ system to an input. The input might be an injected radioactive tracer of biological activity in nuclear medicine imaging procedures, or a pulse sequence in nuclear magnetic resonance studies. Over the past years the major focus of research in physiologic studies employing tracers has been the accurate measurement of the response of the biological system and the related technological developments of emission tomography. In addition, attention has been directed toward computer implementation of mathematical methods of kinetic modeling for extracting the desired physiological parameters from tomographically derived data. Recently, these efforts have uncovered the importance of accurate characterization of the input function and limitations imposed by statistical uncertainty of the data on the type and number of parameters which can be extracted from an observation (1).

The method presented here uses the estimate of the statistical uncertainty of observed data (represented by the data covariance matrix), together with the expected variation of observations predicted by the kinetic model due to small changes in the model parameter values (represented by a sensitivity matrix) (2). For a given model the sensitivity matrix, as well as the data covariance matrix, will depend on the shape of the input function and the frequency of observation. For example a flat input function or a low sampling rate will lead to observed data which are insensitive to rapid physiological processes. The sensitivity matrix and the data covariance matrix are used to generate the parameter covariance matrix. It is the determinant of this parameter covariance matrix which we use to measure the optimality of the experimental design. Since this determinant is proportional to the volume of the n-dimensional parameter estimate confidence region, the smaller the determinant the better the input and sampling strategies. We will refer to this confidence region as the uncertainty elipsoid.

The method we present is of general applicability for any model in computed tomography studies, as the form and values of the sensitivity matrix depend on the definition of the model, and the data covariance matrix is defined by the actual data uncertainties which can be estimated by the data acquisition technique (3). In this paper we compare a range of sampling and injection protocols in contemporary

use in positron emission tomography (PET) experiments by calculating their relative covariance matrix determinant values. Also examined are effects of neglecting parameters which are necessary to accurately describe the data.

METHODS

PET study model

A dynamic PET experiment can be generalized as follows (see Fig. 1): usually a single intravenous injection of a radionuclide (the input function) is performed, and the time course of the activity in some region of interest in the tomographic slice is recorded. The true input function cannot usually be monitored, and multiple blood samples are analyzed to estimate the time-activity function in the vascular compartment. A mathematical model representing the physiological behaviour of the tracer is then fit to the data in order to estimate the rate constants and their covariance matrix. Unless specified otherwise, the three-compartmental model used in 18-fluorodeoxyglucose (FDG) experiments (4) will be the reference system. To this model we add a vascular fraction f_v. A single-input, single-output experiment (with blood samples and tomographic PET data) will be the reference experimental protocol. A parameter τ is also included in the system in order to account for the time delay between the arrival of tracer at the blood sampling site and the arrival of tracer at the organ studied by PET sampling. The vascular compartment concentration $x_1(t)$ (assumed to be known without error in this work) is the input function of a three compartment system; the concentrations of unphosphorylated and phosphorylated glucose are denoted by $x_2(t)$ and $x_3(t)$, respectively. An analogous treatment can be envisioned for amino acid brain or heart kinetics; however here $x_3(t)$ would represent sequestered label in protein. Equations describing transfer of matter between compartments can be summarized as:

$$\frac{dx_2}{dt} = k_1 x_1(t-\tau) \; - (k_2 + k_3) x_2(t) \; + k_4 x_3(t) \; , \tag{1}$$

$$\frac{dx_3}{dt} = k_3 x_2(t) \; - \; k_4 x_3(t) \; . \tag{2}$$

Let $a(t)$ be the activity in the region of interest:

$$a(t) = s \left\{ f_v x_1(t-\tau) + (1 - f_v) \left[x_2(t) + x_3(t) \right] \right\} \; , \tag{3}$$

where s is concentration-activity scaling factor, f_v is the fractional volume of tissue comprising blood capillaries, and τ is the sample delay time which depends on the blood sampling site and method (e.g. a long catheter has a corresponding large τ).

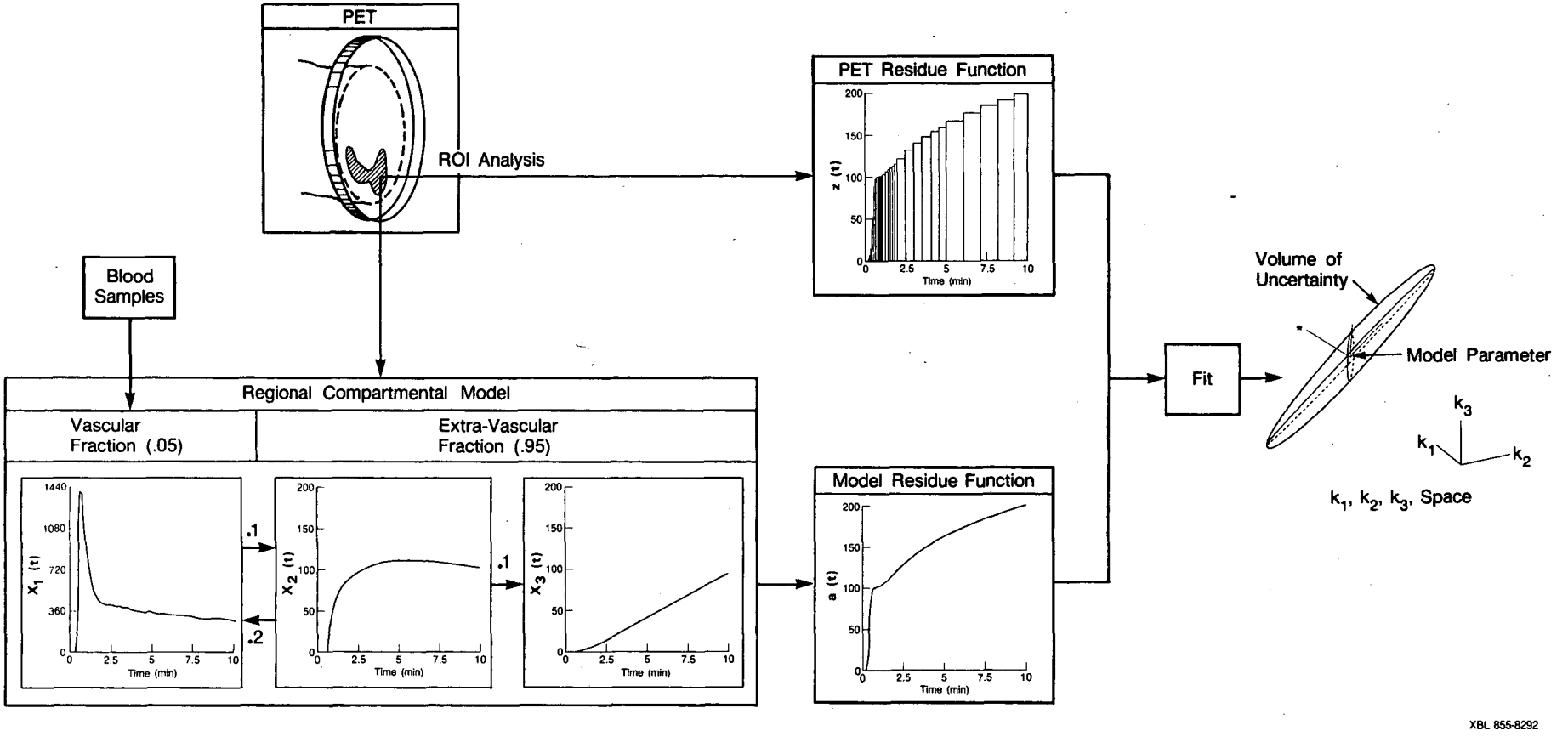

Fig. 1 Flow-chart of a dynamic FDG-PET experiment. The fit provides estimates of the compartmental model parameters and of their accuracies in terms of a covariance matrix. On the right is the uncertainty elipsoid corresponding to the covariance matrix of k_1, k_2 and k_3.

Solving the system of differential equations gives:

$$a(t) = s\left[f_v x_1(t-\tau) + (1-f_v)(h * x_1)(t)\right] , \tag{4}$$

where "$*$" denotes the convolution operator,

$$(h * x_1)(t) = \int_{-\infty}^{t} h(t-s)x_1(s-\tau)ds , \tag{5}$$

and "h" is the impulse response of this system,

$$h(t) = \alpha_1 e^{-\lambda_1 t} + \alpha_2 e^{-\lambda_2 t} , \tag{6}$$

with α_i and λ_i defined as (5):

$$\lambda_i = \frac{k_2 + k_3 + k_4 \pm \sqrt{(k_2+k_3+k_4)^2 - 4k_2k_4}}{2}, \; i = 1,2 , \tag{7}$$

$$\alpha_i = \pm k_1 \frac{k_3 + k_4 - \lambda_i}{\sqrt{(k_2+k_3+k_4)^2 - 4k_2k_4}}, \; i = 1,2 . \tag{8}$$

The tomographic device provides a series $(y_j,\ j = 1,2,..n)$ of measures of mean values of $a(t)$ over time intervals (t_{j-1}, t_j), but y_j is usually assumed to be equal to $a(\frac{t_{j-1}+t_j}{2})$. As noticed by previous authors (6), sample concentrations at the midpoint are not accurate mean values for time varying activities and can generate biased parameter estimates. Clearly, unbiased parameter estimates are desirable, and therefore we use a true integral model (instead of a simple first order correction as proposed in the reference cited above). The effects of using a non-integral model are also investigated in this paper. The integral model value for y_j is given by:

$$y_j = \frac{1}{t_j - t_{j-1}} \int_{t_{j-1}}^{t_j} a(t)dt , \; j = 1,2,...,n . \tag{9}$$

We assume that a(t) is a continuous non-homogeneous Poisson process (7) and we approximate experimental uncertainty on the y_j values $(e_1, e_2, \ldots, e_n)$ as an n-variate normal distribution $N(\{\mu_i = 0\},\ \|\sigma_{ij}\|)$, where $\Sigma = \|\sigma_{ij}\|$ is the covariance matrix of the data z_j $(z_j = y_j + e_j)$.

Notice that the whole process can be interpreted in terms of linear time-invariant systems and can be formalized as follows (8):

$$\frac{d\mathbf{x}}{dt} = A(\mathbf{p})\mathbf{x}(t) + B(\mathbf{p})\mathbf{u}(t-\tau) , \tag{10}$$

$$\mathbf{y}(t) = C(\mathbf{p})\mathbf{x}(t) + D(\mathbf{p})\mathbf{u}(t-\tau),\ 0 \le t \le T , \tag{11}$$

$$\mathbf{z}_j = \mathbf{y}(t_j) + \mathbf{e}_j,\ j = 1,2,...n , \tag{12}$$

where $\mathbf{x}$ denotes the vector of state variables (concentration or mass in the compartments), $\mathbf{u}$ is the input function vector, $\mathbf{y}$ the output vector, $\mathbf{z}_j$ the measurements of $\mathbf{y}$ at the discrete time t_j (with some uncertainty $\mathbf{e}_j$). A, B, C and D are matrices depending on the model parameter vector $\mathbf{p}=(k_1, k_2, k_3, k_4, f_v, \tau)^T$, T is the total time of the study, and n is the number of samples. For the reference system described above:

$$A = \begin{pmatrix} -(k_2+k_3) & k_4 \\ k_3 & -k_4 \end{pmatrix}, \; B = (k_1), \; C = (1-f_v, 1-f_v), \; D = (f_v) \; . \qquad (13)$$

Parameter and covariance matrix estimation

Using any of the available procedures to fit $\mathbf{y}$ to $\mathbf{z}$ will provide a parameter vector estimate $\hat{\mathbf{p}}$. Two kinds of information are useful in order to assess the quality of this estimate: the bias in its mean,

$$\mathbf{b} = E(\hat{\mathbf{p}}) - \mathbf{p} \; , \qquad (14)$$

and its covariance matrix,

$$COV(\hat{\mathbf{p}}) = E\{(\hat{\mathbf{p}} - E\{\hat{\mathbf{p}}\})^2\} \; , \qquad (15)$$

where $E\{.\}$ stands for the mathematical expectation of a random variable.

Parameter biases resulting from using the non-integral model were computed by fitting the a values at the mid-intervals (see Eq. 4) to data generated using the integral model. In order to evaluate biases in parameter estimates resulting from assigning wrong constant values to f_v and τ instead of including these two parameters in the estimation process, fits were also performed with various constant values for these two parameters.

The covariance matrix of $\hat{\mathbf{p}}$ as defined in Eq. 15 gives a measure of the precision of $\hat{\mathbf{p}}$. A general (but extremely cumbersome) method to estimate $COV(\hat{\mathbf{p}})$, is to do a Monte-Carlo simulation of the experiment (for example generate 1000 data sets, obtain 1000 estimates of $\mathbf{p}$, and compute the covariance matrix from this sample). Fortunately, for models that are linear in the parameters (e.g. $\mathbf{y} = S\mathbf{p}$), $COV(\hat{\mathbf{p}})$ is easy to compute for least-squares estimates. Moreover, if the data errors (Σ) are used as weights for the least-squares fit, $\hat{\mathbf{p}}$ is the minimum variance unbiased estimate (Gauss-Markov theorem) and its covariance matrix is given by:

$$COV(\hat{\mathbf{p}}) = (S^T \Sigma^{-1} S)^{-1} \; . \qquad (16)$$

(Notice that for normally distributed data, Gauss-Markov and Maximum Likelihood estimation are identical (9).) Equation 16 clearly shows how the data errors are propagated in the parameter estimate uncertainties through the matrix S. Note that S, the sensitivity matrix, is the derivative of $\mathbf{y}$ with respect to $\mathbf{p}$.

More often than not, non-linear models must be used to describe correctly the physiological process and the measurement process of the experiment (as it is the

case for the multi-compartment model described above). The determination of the parameter covariance matrix as defined by Eq. 16 can be extended to non-linear models. Let $S = (s_{ij})$ still denotes the sensitivity matrix (the derivative of **y** relative to **p**, which now depends on **p**):

$$s_{ij} = \frac{\partial y_i}{\partial p_j},\ i = 1, 2, ..., n,\ j = 1, 2, ..., r\ , \tag{17}$$

where r equals the number of parameters; s_{ij} represents the variation in the i^{th} observation due to a unit variation of p_j. If S is computed at the true value of **p**, if the data are Gaussian and if a Gauss-Markov criterion is used, equation 16 is a good approximation of the actual parameter estimate covariance matrix (9).

PET data simulation and analysis

Comparison of various experimental designs requires an initial dataset from which the data relative to the various protocols can be generated. To provide a function used for the standard or reference input data ($x_1(t)$ in counts per ml per minute) patient data were acquired. Following a fast venous injection into the arm of a patient (2 second injection duration), blood samples were drawn (at 5 to 7 sec intervals for the first minutes of the experiment), counted in a well counter and scaled to tomographic data using a conversion factor of well-counter to PET events per volume (10).

Given a set of values for $\mathbf{p} = (.1\ min^{-1}, .2\ min^{-1}, .1\ min^{-1}, 0.\ min^{-1}, .05, 10\ sec)^T$, we generated y_i^* values using Eq. 4 and 9 on a one second time scale (superscript * stands for 1 sec duration data file) using a discrete convolution algorithm (11). Back transport from the third compartment (represented by k_4) was not used in this study, as previous work (1) had pointed out that its determination is not warranted in dynamic PET-FDG brain experiments lasting less than 40 min.

Given the sequence of t_j (the sampling protocol), a PET dataset (z_j) is created by adding a weighted sum of these y_i^* (the integral model y_j value) and, when required, a noise contribution (e_j) using a Gaussian pseudo-random number generator:

$$\left.\begin{array}{c} z_j = y_j + e_j \\ y_j = \frac{1}{(t_j - t_{j-1})} \sum_{i=t_{j-1}}^{t_j} y_i^* \\ e_j = N(0, \|\sigma_{ij}\|) \\ \sigma_{ij}^2 = \delta_{ij} \frac{y_j}{(t_j - t_{j-1})} \end{array}\right\} i, j = 1, 2, ..., n\ , \tag{18}$$

where δ_{ij} is the Kronecker delta function. The z_j are assumed to be uncorrelated, e.g. Σ is diagonal with elements σ_{jj}^2.

Different sampling protocols have been tested (see Fig. 2 and Table 1), some of which are currently used by various groups. We tested protocols with the same total time, T, and various sampling rates, as well as protocols with different total time and similar sampling rates. Also, a set of blurred input functions (and the corresponding residue functions) were generated by convolving the reference input

function with unit area rectangular functions of durations 10, 30, 60 and 120 sec. These blurred input functions are used to evaluate the effects of prolonging the intravenous injection. Figure 3 shows the reference input function, the input function for the 120 sec duration injection and their corresponding model residue functions ($y(t)$). For each set of input function and sampling strategy we fit the various models (integral and non-integral, with f_v and τ included in the fit parameter list or set to wrong constant values) to the PET dataset using a Marquardt-type (12) optimization method and a Gauss-Markov criterion. The fitting procedure minimizes a χ^2 statistic:

$$\chi^2 = \sum_{j=1}^{n} \left(\frac{z_j - y_j}{\sigma_{jj}}\right)^2 . \tag{19}$$

From Eq. 4, 5 and 9, it is clear that fitting the integral model requires the computation of a double integral for each time point at each iteration, which is very time consuming. Therefore, we designed an algorithm to speed up this part of the estimation process (see appendix A) and validated it before proceeding with the simulation analyses. Estimation of the parameter covariance matrix has been achieved numerically using Eq. 16, where each term s_{ij} of the matrix S defined in Eq. 17 is evaluated using a central difference operator:

$$s_{ij} = \frac{y_i(p_j + \Delta p_j) - y_i(p_j - \Delta p_j)}{2\Delta p_j} ; \tag{20}$$

Δp_j is a small increment of the p_j parameter value.

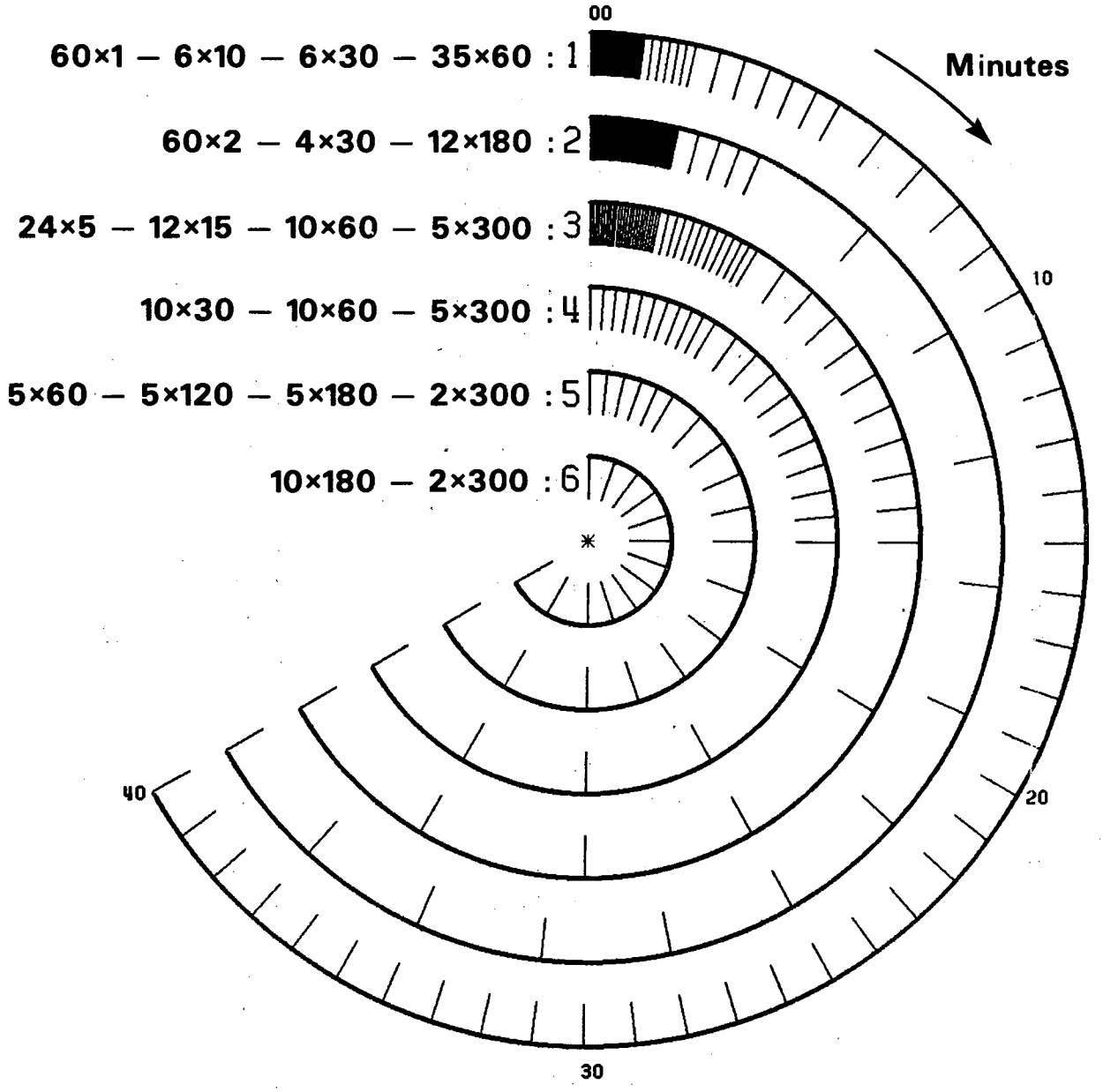

XBL 855-8290

Fig. 2 Various sampling protocols, some of which are currently used in FDG-PET experiments, are compared in this work. In all cases tomographic data are acquired continuously and what differs are the durations and number of images, e.g. Protocol 1 has 60 images at 1 sec. intervals followed by 6 images at 10 sec. intervals, then 6 images at 30 sec. intervals and 35 images at 60 sec. intervals.

Table 1. *Sampling strategies with various study durations (T)*

Initial frame duration (sec)	Sampling strategy (nr of frames x frame duration)	Study duration T (sec)
1	95x1 - 12x2	119
	60x1 - 6x10 - 31x6	306
	60x1 - 6x10 - 6x30 - 35x9	615
	60x1 - 6x10 - 6x30 - 35x26	910
	60x1 - 6x10 - 6x30 - 35x43	1505
	60x1 - 6x10 - 6x30 - 35x60	2400
	60x1 - 6x10 - 6x30 - 35x77	2995
	60x1 - 6x10 - 6x30 - 35x94	3590
30	6x30	180
	10x30	300
	10x30 - 5x60	600
	10x30 - 10x60	900
	10x30 - 10x60 - 2x300	1500
	10x30 - 10x60 - 5x300	2400
	10x30 - 10x60 - 5x300 - 1x600	3000
	10x30 - 10x60 - 5x500 - 2x600	3600
180	5x180	900
	7x180	1260
	9x180	1620
	10x180	1800
	10x180 - 1x300	2100
	10x180 - 2x300	2400
	10x180 - 1x400	3000
	10x180 - 6x300	3600

The initial frame durations are kept constant for each of the three group of protocols, and correspond to the initial sampling rates of protocols 1, 4 and 6 of Fig. 2.

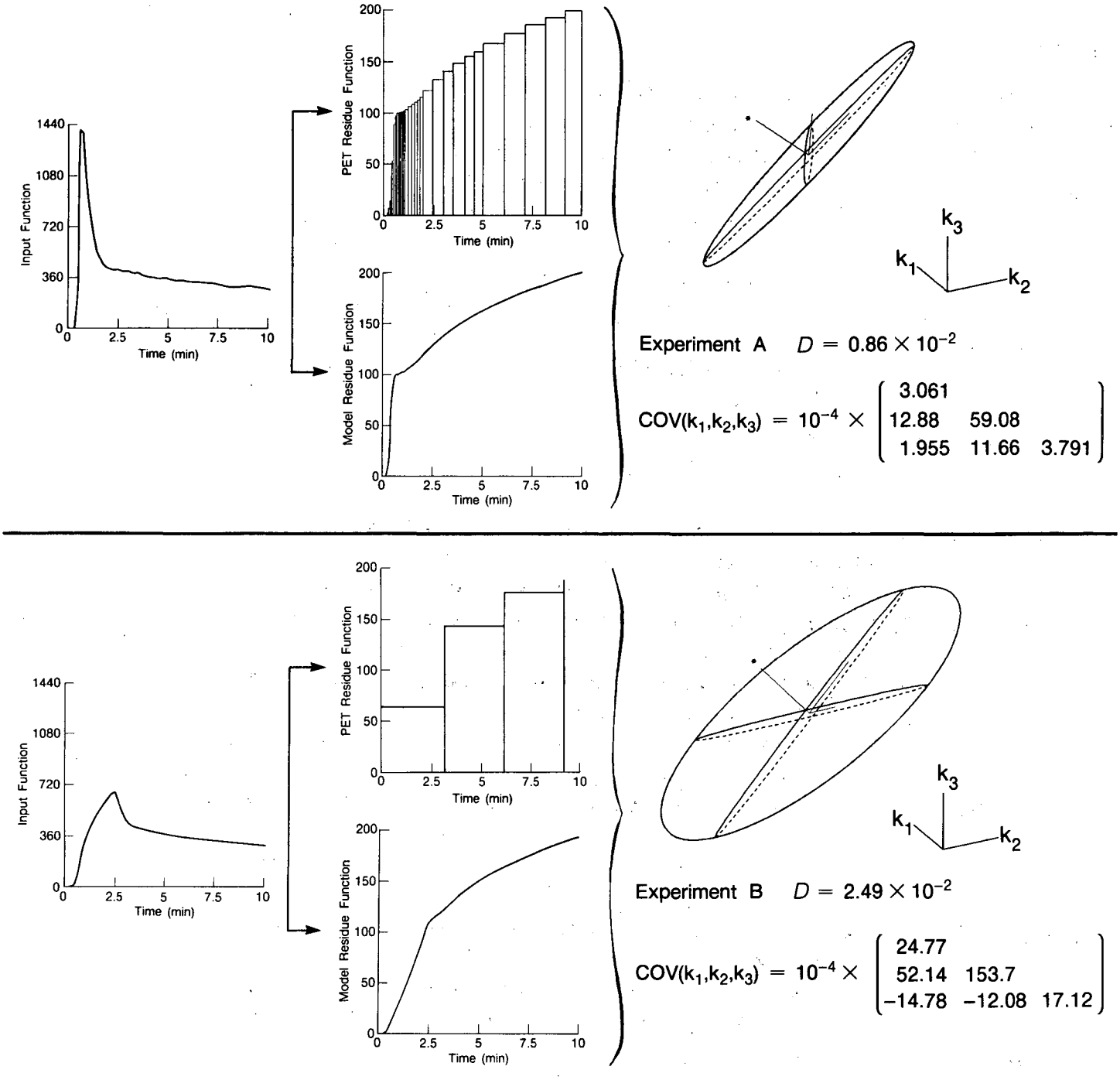

Fig. 3 Comparison of two FDG-PET experimental designs with different sampling strategies and input functions. A fast injection and 1 sec initial frame duration are used in experiment A, and a 120 sec injection and 180 sec initial frame duration in experiment B. On the right are shown the actual covariance matrix of the parameters k_1, k_2, k_3, the corresponding uncertainty ellipsoid and its normalized volume D for both protocols.

Protocol comparison

The parameter covariance matrix gives the precision on the parameter estimate. In addition to its dependence on the fitting procedure, equations 10-12 clearly show that $COV(\hat{\mathbf{p}})$ also depends on experimental factors such as the input function shape (u) and the data collection strategy (the series and number of t_j), over which the investigator has control. The magnitude of some scalar function of this matrix, such as its determinant (a quantity proportional to the volume of the parameter confidence region (2,13))provides a criterion for discriminating between various experimental protocols. This measure of protocol optimality, known as D-optimality in the case of minimizing $det(COV(\hat{\mathbf{p}}))$, has been proposed in other fields of research (2,13-15), where it is often referred to as the information matrix approach. Minimizing the determinant of $COV(\hat{\mathbf{p}})$ is equivalent to maximizing the determinant of the matrix M defined as:

$$M = COV(\hat{\mathbf{p}})^{-1} = S^T \Sigma^{-1} S \ . \tag{21}$$

The matrix M may be interpreted as the information contained in the data relative to the fact that we try to estimate $\mathbf{p}$. A property of the information matrix, M, is that the diagonal elements of its inverse are the lower bound of any unbiased parameter estimate variances (16) or, more generally, that the ellipsoid relative to M^{-1} lies inside any unbiased parameter estimate uncertainty ellipsoid (9). Thus, the determinant of M provides a measure of the maximum global achievable accuracy of the parameter estimate for a given experimental protocol.

However, the principal parameters of interest in dynamic PET-FDG experiments are the rate constants k_1, k_2, k_3, because they represent the physiological process under study. In addition, the local glucose metabolic rate (4) is proportional to the ratio ($\mathcal{R}$) given by:

$$\mathcal{R} = \frac{k_1 k_3}{k_2 + k_3} \ . \tag{22}$$

The parameters f_v and τ are necessarily included in the model because of the nature of the data acquired in PET experiements, but they do not contain significant information about the local brain glucose metabolism. For these reasons, as a measure of merit for the various protocols and input functions we shall use the determinant (Δ) of the covariance matrix of only k_1, k_2 and k_3. Because $\mathbf{p}$ also includes f_v and τ, this matrix is a submatrix of $COV(\hat{\mathbf{p}})$. Recall that the determinant of this submatrix is not the quantity which is minimized in a fit for a given protocol, but instead is a measure of the precision that can be obtained on the estimated k's using this protocol. In subsequent figures we will plot a normalized value of this quantity denoted by $\mathcal{D}$, and defined as:

$$\mathcal{D} = \left(\frac{\Delta}{(k_1 k_2 k_3)^2} \right)^{1/6} \ . \tag{23}$$

$\mathcal{D}$ can be interpreted as a mean coefficient of variation for the k's. For uncorrelated parameters, $\mathcal{D}$ is actually the geometric mean of the parameter coefficients of

variation:

$$D = \left(\frac{\sigma_{k_1}}{k_1}\frac{\sigma_{k_2}}{k_2}\frac{\sigma_{k_3}}{k_3}\right)^{1/3} . \quad (24)$$

Such a criterion, when all of the fit parameters are not of interest, has been previously proposed (2). A comparison of two protocols is shown in Fig. 3.

RESULTS

Effects of rate of injection and rate of data collection

Effects of various sampling rates at early times after injection on parameter estimate precision are shown on Fig. 4; the reference curve and the corresponding residue function have been used for this particular set of results. We plot D, the normalized determinant of the covariance matrix of k_1, k_2, k_3 as well as the three individual parameter estimate coefficients of variation, as a function of the initial image duration for each of the six sampling protocols shown in Fig. 2. A second set of figures (Fig. 5a,b,c,d) decribes the effects of T, the total time of the study, for three different protocols (1,4,6). For each protocol, the initial frame duration is kept constant while additional information is added using later images. Effects of increasing the injection duration are shown in Fig. 6 for each sampling protocol. Notice that an optimal input function seems to exist for some protocols.

Effects of using a non-integral model

In order to show the discrepancies between the true residue function (generated using the integral model described in Eq. 9 and the residue function $y(t)$ computed using a value at the mid time-interval, we plotted these curves for various sampling protocols in Fig. 7. Notice that these discrepancies are clearly dependant on the sampling rate at early times. Fitting these residue functions to data generated using the integral model provided biased parameter estimates whose dependence on the sampling rate at early times and increasing injection durations is shown is Table 2.

Effects of fixing some parameters

Fitting the PET data using a reduced number of fit parameters and constant true values for the others reduces the discrepancies between the various protocols found in the previous section as shown in Fig. 8. In addition, the precision of parameters is usually better since fewer parameters are fit, but this effect is minimized in the sampling protocols using fast initial sampling rates. However, important biases which depend on the experimental design are generated for the fit parameters when wrong values are used for the parameters not fit. The bias values can be predicted using a first order expansion of the χ^2 criterion (see appendix B) and the Table 3 gives the first order derivatives of the parameter k_1, k_2, k_3 considered as functions of the parameters f_v and τ.

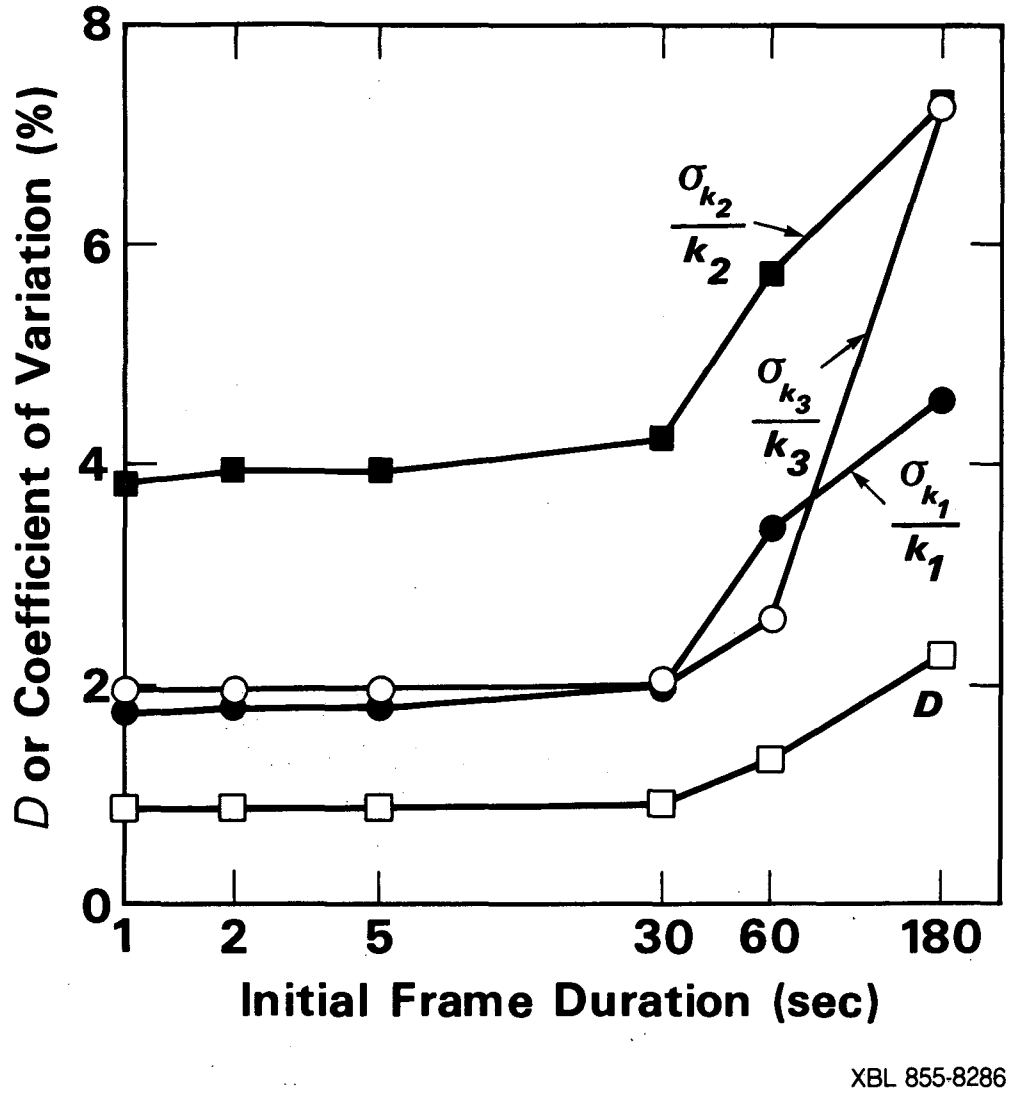

Fig. 4 Comparison of experiments using the same reference input function and the six different sampling protocols of Fig. 2 distinguished by their initial frame durations on the abscissa: normalized determinant of k_1, k_2, k_3 covariance matrix ($\mathcal{D}$ (⊔)), and individual coefficients of variation (k_1 (○), k_2 (⊔), k_3 (•)).

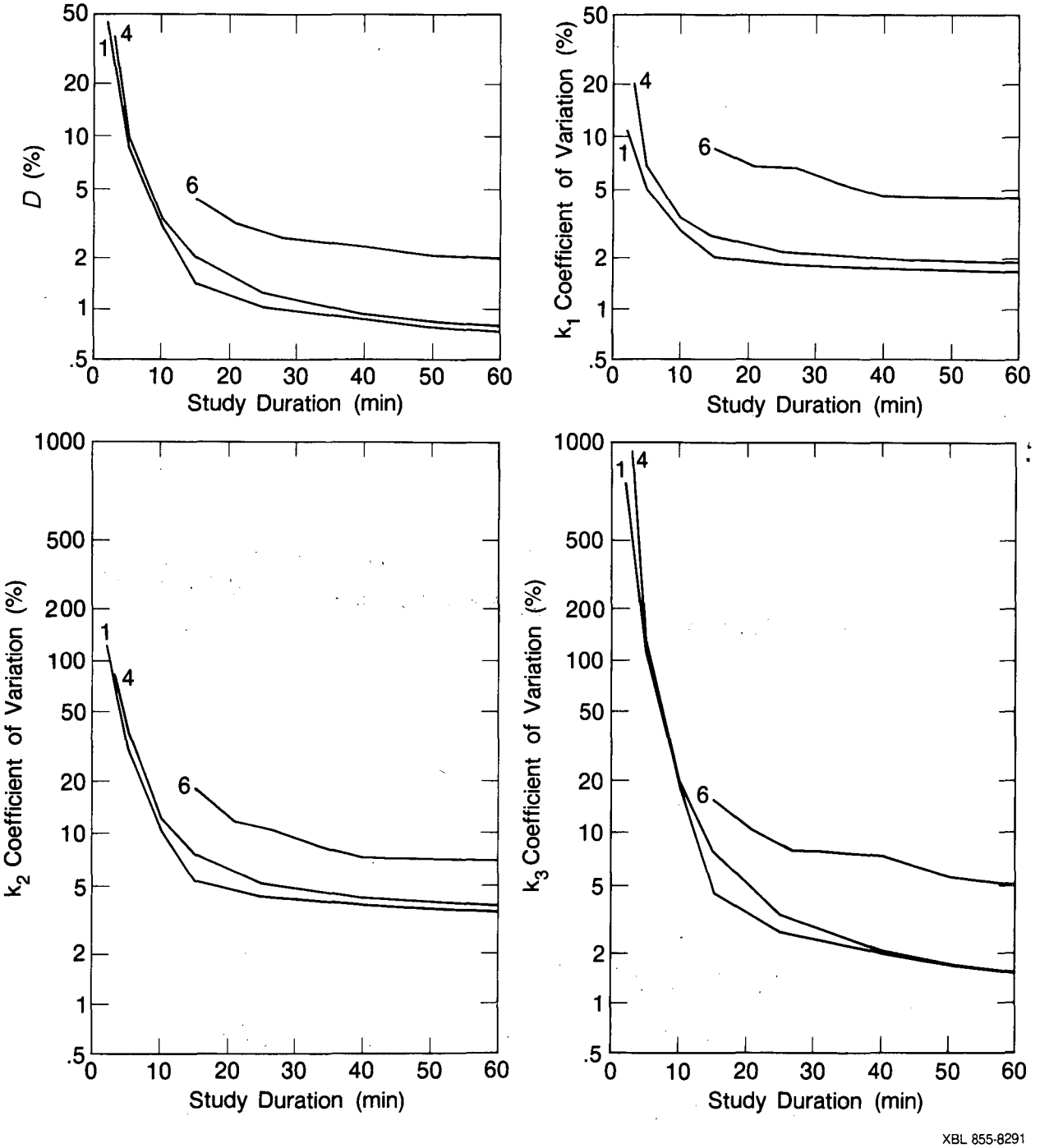

Fig. 5 Comparison of experiments using the reference input function and initial frame durations of protocols 1, 4 and 6 of Fig. 2 (1, 30, and 180 sec respectively) as a function of the study duration T; **a**: normalized determinant of k_1, k_2, k_3 covariance matrix (D);
b,c,d: coefficient of variation of k_1, k_2 and k_3 respectively.

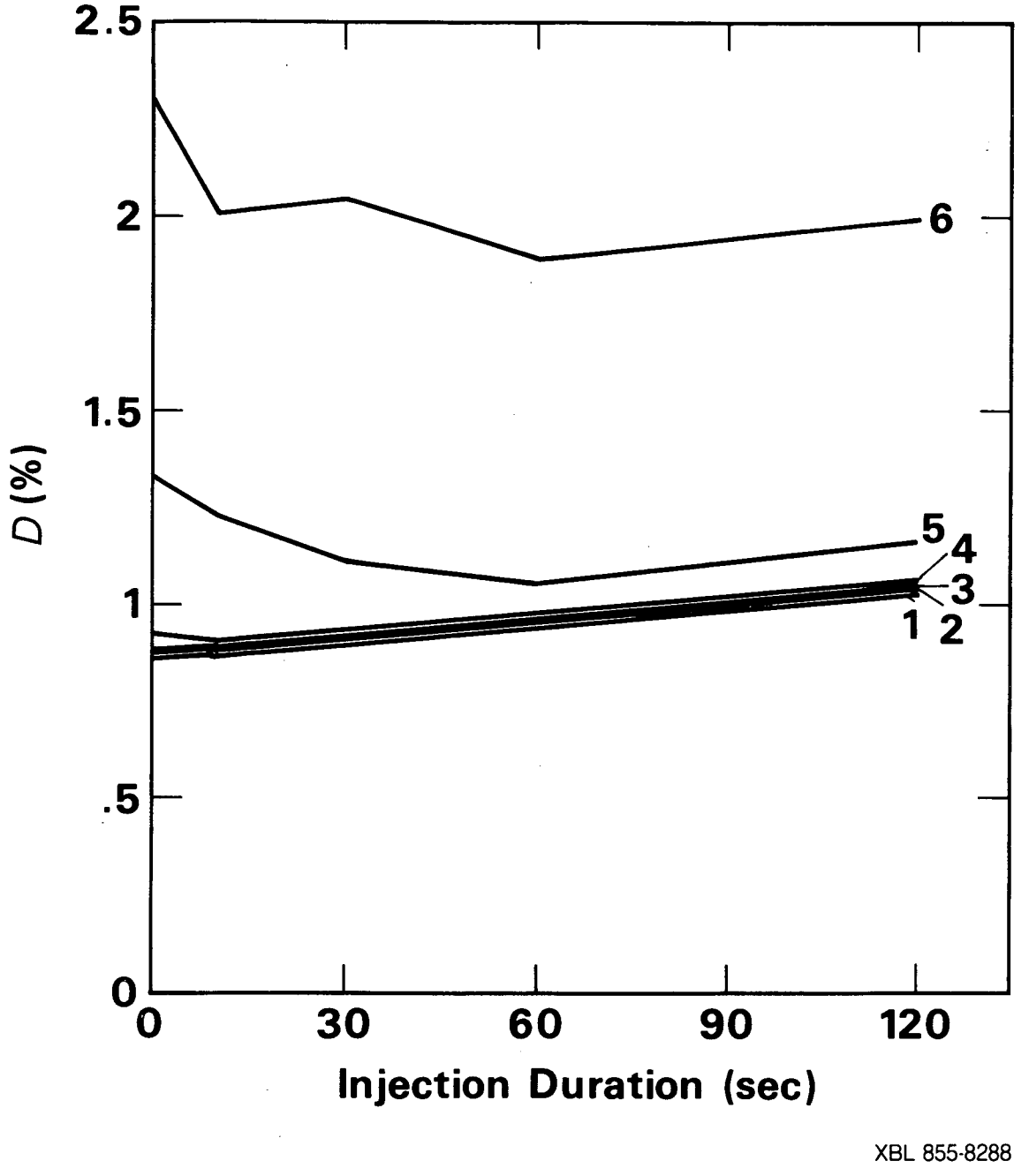

Fig. 6 Comparison of experiments using the six different sampling protocols of Fig. 2 as a function of the injection duration: normalized determinant of k_1, k_2, k_3 covariance matrix ($\mathcal{D}$).

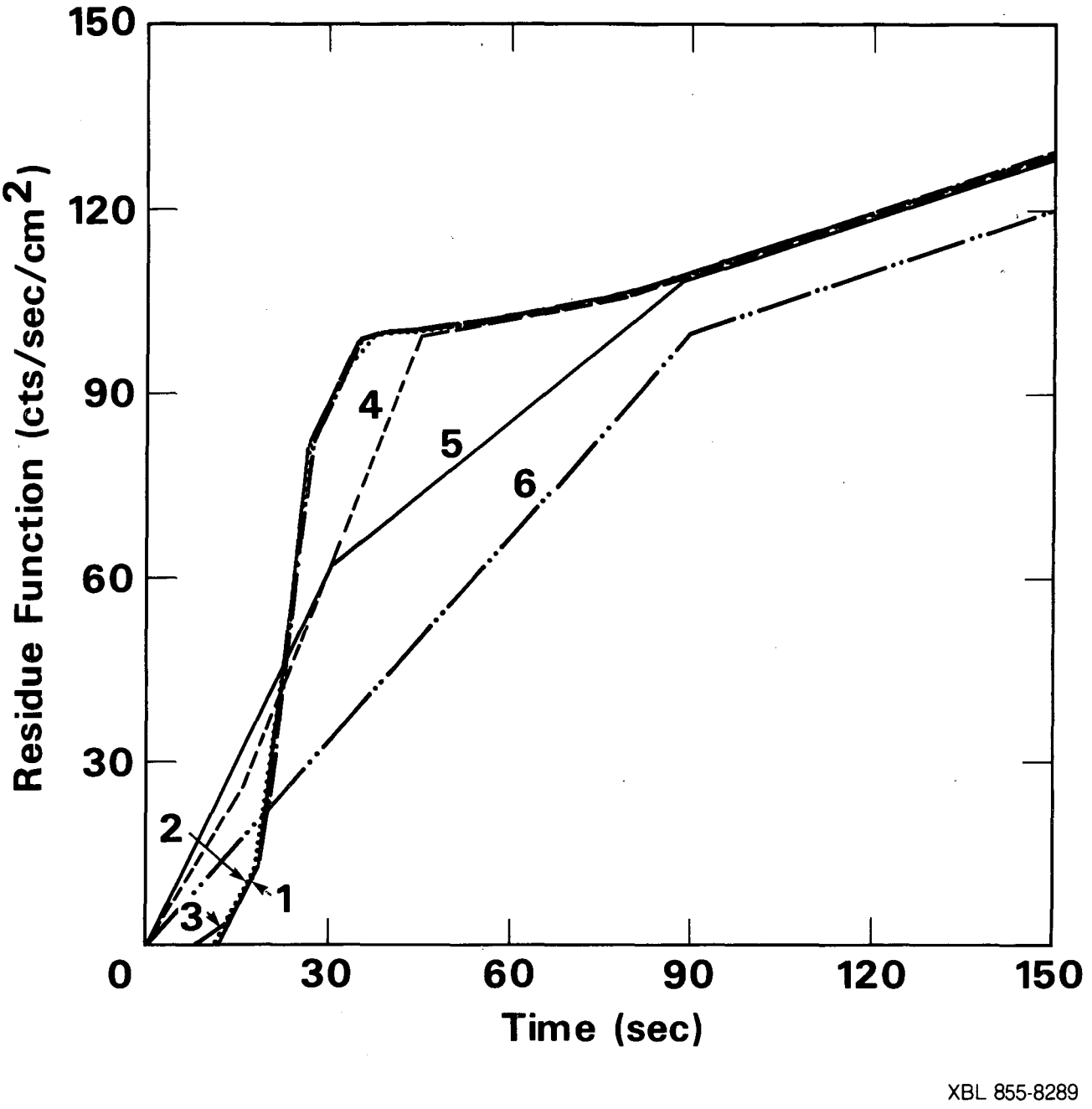

Fig. 7 Residue function for six experiments using the sampling protocols of Fig. 2 and the reference input function. The residue function is computed at the mid-point of each image time interval by using its mean value over this interval.

Table 2. *Biases (in % of the parameter true value) in the mean of parameter estimates and* $\mathcal{R} = \frac{k_1 k_3}{k_2 + k_3}$ *resulting from the use of a non-integral model.*

parameter	sharp input function			blurred input function		
	prot 1	prot 4	prot 6	prot 1	prot 4	prot 6
k_1	.02	1.7	9.9	.002	5.7	7.3
k_2	.002	2.8	11.4	.003	9.3	10.
k_3	.005	.32	7.	.04	1.7	9.3
f_v	.6	1.3	62.	.01	34.	94.
t_o	.06	50.	100.	.08	67.	170.
$\mathcal{R}$	.01	.11	3.	.004	1.5	5.4

Values were obtained by fitting the non-integral model using two different input functions (the sharp reference and a blurred function obtained by convolving the reference with a unit area rectangular function of 60 second duration), and three PET data protocols (1, 4 and 6 of Fig. 2 with initial frame duration 1, 30 and 180 sec). Notice that since a one second time scale was used to generate the data, no significant biases are observed for protocol 1 (sampling rate=1/sec).

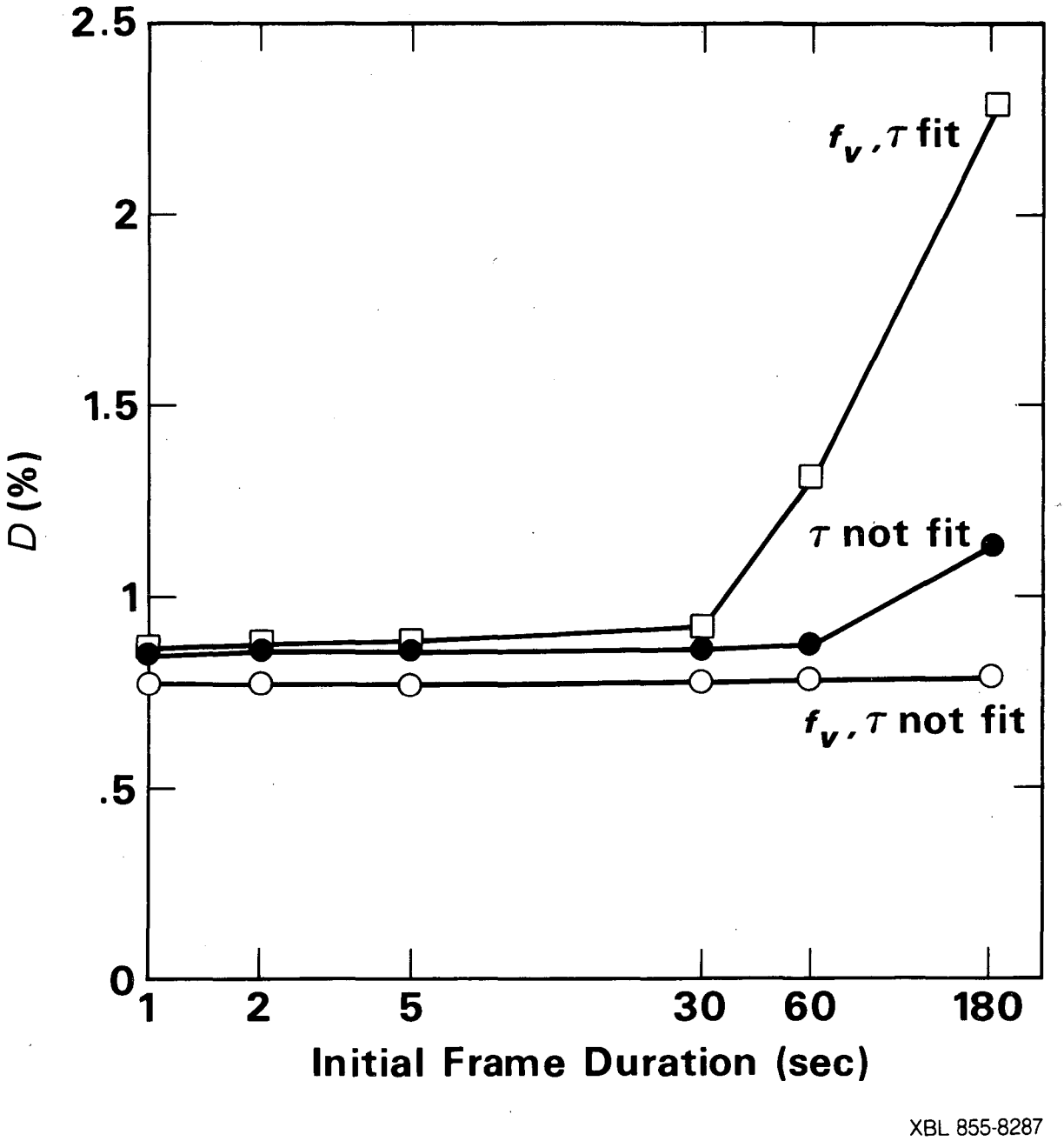

Fig. 8 Comparison of experiments using the six different sampling protocols of Fig. 2 and the same reference input function, when some model parameters are not fit but set to their true values. This figure demonstrate the effect of including or excluding parameters such as the delay between the arrivals of the tracer at the blood and PET sampling sites (τ) and the vascular fraction (f_v) on normalized determinant of k_1, k_2, k_3 covariance matrix (D).

Table 3. *Normalized partial derivatives of fit parameters* (k_1, k_2, k_3) *and* $\mathcal{R} = \frac{k_1 k_3}{k_2 + k_3}$, *relative to constant parameter* f_v *and* τ.

	sharp input function A		
	protocol 1	protocol 4	protocol 6
$\frac{f_v}{k_1}\partial k_1/\partial f_v$	-.33	-.34	-.38
$\frac{\tau}{k_1}\partial k_1/\partial \tau$	.059	.067	.12
$\frac{f_v}{k_2}\partial k_2/\partial f_v$	-.61	-.64	-.7
$\frac{\tau}{k_2}\partial k_2/\partial \tau$	.11	.13	.25
$\frac{f_v}{k_3}\partial k_3/\partial f_v$	-.065	-.07	-.085
$\frac{\tau}{k_3}\partial k_3/\partial \tau$	.028	.036	.076
$\frac{f_v}{\mathcal{R}}\partial \mathcal{R}/\partial f_v$	.033	.032	.033
$\frac{\tau}{\mathcal{R}}\partial \mathcal{R}/\partial \tau$	.004	.004	.007

Normalized derivatives (in relative value) are given for protocol 1, 4, and 6 (with initial frame duration 1, 30, 180 sec respectively, see Fig. 2) and the sharp reference input function. These derivatives can be used to predict the bias of fit parameter estimates when using wrong constant values for other parameters as proved in Appendix B. For example setting f_v to .04 instead of .05 and τ to 11 instead of 10 sec will generate a value of k_1 overestimated by 7.2% $(-20\% \times .33 + 10\% \times .059)$ for protocol 1.

Notice the sensitivity of the parameters k_1 and k_2 to small changes of f_v, and the cancellation of these sensitivities when the ratio $\mathcal{R} = \frac{k_1 k_3}{k_2 + k_3}$ is computed. This stability of $\mathcal{R}$ (previously noticed by different authors (4,5)) appears on the uncertainty elipsoids of Fig. 1 and 2. The gradient of $\mathcal{R}$ with respect to $(k_1, k_2, k_3)^T$ is very close to the linear combination of the k's that has the smaller uncertainty. This linear combination is represented by the elipsoid axis labeled by a "*" on Fig. 3.

DISCUSSION

It may have been noticed on Fig. 4 and 5, that the shape of the curve of $\mathcal{D}$ (the normalized covariance matrix determinant) is similar to the shape of the individual k coefficient of variation curves, and therefore, unless otherwise specified, results will be discussed with reference to this quantity only. $\mathcal{D}$ is a good parameter space criteria because it is invariant under scale changes in the parameters or linear transformation of the ouput, properties that other proposed global criteria such as a weighted trace (an average of the parameter estimate variances) do not fulfill (13). The validity of our results relies on the fact that when the true data uncertainties are used in the Gauss-Markov estimation, equation 15 provides a good estimate for $COV(\hat{\mathbf{p}})$. In one simulation, we checked the validity of this asumption: we generated 1000 sets of data (y) using the reference input function, sampling protocol 4 (see Fig. 2) and a Gaussian pseudo-random number generator for the noise. Each of these sets was fit, and Table 4a compares the observed covariance matrix of the estimates with the matrix computed using Eq. 15 and the true value of the parameters. These matrices are very close. The same simulated data were fit to the non-integral model and experimental biases are compared to those obtained when fitting non-noisy data in Table 4b, showing a very good agreement. Table 4b provides an estimate of the order of magnitude of the precision of our results. We found that two-sided derivatives (see Eq. 17) are necessary in the fitting process in order to obtain this precision, because single-sided derivatives give erratic behavior near the minimum. Our model for the FDG experiment is a combination of a well-known model for the FDG pathway in the brain (4) and of a model of data collection and noise using PET. It has been shown by different authors that for the practical time course of an FDG-PET experiment, this model is sufficient (1). However the methodology holds for studying more complicated models of other biological systems. Also of practical importance is to include the parameters f_v and τ in this model. Use of constant values for these parameters is unrealistic, and Table 3 has shown that, especially for protocols with fast sampling, large biases are generated for parameters strongly correlated with early time data. It should be emphasized that, for all the protocols, assuming that the fitting algorithm is provided good starting values, unbiased parameter estimates are obtained using the integral model. However, our results show that the precision as well as the sensitivity of the fit is highly dependent on the relationship between the sampling rate and the

frequency components of the residue function $y(t)$ during the experiment.

Table 4a. *Precision study results for the integral model.*

parameter	sample mean	sample standard error ($x10^3$)
k_1 (min^{-1})	.10006 (.10000)	1.9729 (1.9599)
k_2 (min^{-1})	.20015 (.20000)	8.5174 (8.4868)
k_3 (min^{-1})	.099919 (.10000)	2.0116 (1.9952)
f_v	.04990 (.05000)	2.3783 (2.3536)
τ (sec)	10.003 (10.000)	449.77 (449.06)
χ^2	19.811 (20.000)	6430.0 (6324.6)

1000 residue functions were generated using the reference input function and a Gaussian pseudo-random generator. Protocol 4 of Fig. 2 (initial frame duration 30 sec) was used to generate 1000 related set of PET data and the integral model was fit to these data, providing a sample of 1000 parameter estimates and χ^2, whose mean value and standard error are compared with their theoretical values (in parentheses). The theoretical values for the standard errors were calculated from Eq. 16, and the theoretical value for the χ^2 is the number of degrees of freedom (number of data points for protocol 4 minus number of fit parameters, $25 - 5 = 20$).

Table 4b. *Precision study results for the non-integral model.*

parameter	true value	sample mean	theoretical value
k_1 (min^{-1})	.1	.09842	.09833
k_2 (min^{-1})	.2	.19501	.19481
k_3 (min^{-1})	.1	.09958	.09967
f_v	.05	.04921	.04933
τ (sec)	10.	15.158	15.141

1000 residue functions were generated using the reference input function and a Gaussian pseudo-random generator. Protocol 4 of Fig. 2 (initial frame duration 30 sec) was used to generate 1000 related set of PET data and the non-integral model was fit to these data, providing a sample of 1000 parameter estimates, whose mean value are compared with their theoretical values obtained using a fit of the non-integral model to data without noise.

For a given parameter vector and input function, it is easy to see that the gain in precision for parameter estimates relies on an a high sampling rate when the residue function y has high frequency components, thus avoiding aliasing problems that may propagate all through the estimation process. Figure 4 emphasizes this result: keeping the total time constant so that the total amount of information available in the experiment is constant, it is easy to see that precision is lost when the initial sampling rate becomes slower. It may be argued that observed differences for parameter precision are a consequence of using different number of data points for the various protocols. However, it has to be kept in mind that the same total number of counts is used for all the protocols. Moreover, in an other set of simulations (in which the experiment duration T and the total number of data points n constant were kept constant) we found the same order of magnitude for the differences in parameter precision relative to protocols with various initial sampling rates. Another result of practical interest is to be found in the fact that using low sampling rate protocols makes the fit procedure very sensitive to the starting values of the parameters. An initial guess such as (.8,.18,.12,.04,-8) for protocol 6 causes our fitting procedure to become unstable, whereas it converges to the true parameter values for all other protocols. It is therefore important to consider algorithm stability with respect to starting values when designing such experiments, and it appears that from this particular point of view, it is better to have many points with low statistics than a few points with good statistics.

Meanwhile, the effect of additional information in the protocol obtained by adding new data is clearly demonstrated. After a given time, depending on the parameter value and its function in the model (Fig. 5a), no significant gain in parameter precision is obtained. Assuming that the patient stays in the tomograph during the entire study (in order to avoid problems when repositioning the patient), say 1 hour maximum, it is clear that the numerical identifiability of some parameters for a given region size has to be questioned. For instance it can be shown that even for a one hour protocol the precision that one can expect on the parameter k_4 (.005 in this simulation) will be 30% at best (to be compared with less than 2% for k_1). Notice that precision may be gained for short total time experiments simply by increasing T, but for some protocols, more precision may be gained by using a different sampling strategy.

Simulations with different input functions show that the best results are obtained with the sharpest input function and the fastest sampling rate for a given set of parameters. However, if we consider a given protocol, there exists an optimal input function. This may also be interpreted as an aliasing problem. For a certain protocol and set of parameters, if the input function is too sharp, aliasing occurs on the residue function sampling; if the input function is too smooth, fast components of the biological system will not be measurable. It must be pointed out that for some sampling schedules, the optimal input function may not be achievable because it is too sharp. This is a common problem when using the input function from an intravenous injection, since the initial bolus is dispersed during its transit from the

injection site to the region of interest. For these protocols, however, the fastest injection always gives the best results. In this analysis, no attempt has been made to include effects of precision of x_1. When counted in a well-counter, blood sample activity can be known with a very good precision and errors due to x_1 precision come mostly from the use of venous samples instead of arterial samples. For example assuming that circulation can be roughly modeled as the convolution by a square function, fitting the model with the 10 sec input function to the data generated with the sharp reference input provides a strongly biased parameter estimate (see Table 5). This effect is more important for protocols with faster initial data collection rates, and may be explained by the fact that the model is sensitive to inaccuracies in the input function measurements at early times through the blood contribution (represented in Eq. 4 by $f_v x_1(t-\tau)$). Protocols with lower initial sampling rates are less sensitive to this contribution, because the averaging of the blood contribution over a relatively long time interval makes this average value more stable with respect to the shape of the input function.

Finally, using the integral model instead of the non-integral model is validated in this study. Results conform to the intuitive idea that sampling strategies with larger time intervals generate larger biases for parameter estimates, when fitting the non-integral model to the data. This fact can be related to the large discrepancies generated when the input function or the residue function have high frequencies components as shown in Fig. 7. Our study shows that it is possible to use the integral model in practice if the double integral of Eq. 12 is carefully computed. Therefore, especially for tomographs with a poor time resolution, the integral model should be used.

Table 5. *Biases (in % of the true parameter value) in the mean of parameter estimate due to arm venous blood sampling instead of true capillary sampling.*

parameter	blurred input function A		blurred input function B	
	protocol 3	protocol 4	protocol 3	protocol 4
k_1	4.3	0.6	9.7	3.3
k_2	8.1	1.0	18.	5.5
k_3	0.2	0.1	0.4	0.5
f_v	9.4	3.0	49.	16.
τ	21.	47.	40.	118.

Venous sampling was simulated by convolving the sharp reference input function (assumed to represent the true brain capillary tracer concentration) with unit area rectangular functions of 10 (A) and 30 sec (B) durations. The PET data were generated with the reference residue curve sampled with protocol 3 and 4 (initial frame duration 5 and 30 sec respectively) of Fig. 2.

Appendix A: computation of y_j for the integral model

In our method, no parametrization of the input function $x_1(t)$ is performed (such as a fit to a multi-exponential function), and instead a linear interpolation between the sampling points is used. Since the impulse response of our reference system $h(t)$ is a linear combination of exponentials (Eq. 6), computing y_j as indicated in Eq. 4,5, and 9 requires the evaluation of double integrals such as:

$$I_j = \int_{t_{j-1}}^{t_j} \left[\int_0^t e^{-\alpha(t-s)} x_1(s-\tau) ds \right] dt \ , \ j = 1, \ldots, n \ . \tag{25}$$

Computing I_j using a double quadrature formula at discrete values of t ($t_{j-1} \leq t \leq t_j$) would be an inefficient method, since the integral in brackets would be recomputed for each value of t. Instead of doing this, suppose we want to evaluate I_j using the equally spaced integration nodes:

$$t_{j-1}, t_{j-1}+\Delta t, \ldots, t_j = t_{j-1+n_j \Delta t} \ . \tag{26}$$

Then I_j may be rewritten:

$$I_j = \sum_{i=1}^{n_j} w_i^j \ , \tag{27}$$

with

$$w_i^j = \int_{t_{j-1}+(i-1)\Delta t}^{t_{j-1}+i\Delta t} \left[\int_0^t e^{-\alpha(t-s)} x_1(s-\tau) ds \right] dt \ . \tag{28}$$

Assuming small steps between the integration nodes (in our study $\Delta t = 1$ sec) we can use the mean value theorem to evaluate w_i^j as:

$$w_i^j = \Delta t \int_0^{t_{j-1}+(i-\frac{1}{2})\Delta t} e^{-\alpha(t_{j-1}+(i-\frac{1}{2})\Delta t - s)} x_1(s-\tau) ds \ . \tag{29}$$

Then, dividing the integration interval in two parts gives:

$$w_i^j = e^{-\alpha \Delta t} w_{i-1}^j + \Delta t \int_{t_{j-1}+(i-\frac{3}{2})\Delta t}^{t_{j-1}+(i-\frac{1}{2})\Delta t} e^{-\alpha(t_{j-1}+(i-\frac{1}{2})\Delta t - s)} x_1(s-\tau) ds \tag{30}$$

so finally, w_i satisfies the recursion relations:

$$w_i^j = e^{-\alpha \Delta t} w_{i-1}^j + (\Delta t)^2 \, e^{-\alpha \frac{\Delta t}{2}} x_1(t_{j-1+(i-1)\Delta t} - \tau) \ , \ i = 2, \ldots, n_j \ , \tag{31}$$

$$w_1^j = e^{-\alpha \Delta t} w_{n_{j-1}}^{j-1} + (\Delta t)^2 \, e^{-\alpha \frac{\Delta t}{2}} x_1(t_{j-1} - \tau) \ , \ j = 2, \ldots, n \ , \tag{32}$$

with:

$$w_1^1 = \tfrac{1}{2} (\Delta t)^2 \, e^{-\alpha \frac{\Delta t}{4}} \, x_1(\tfrac{\Delta t}{4} - \tau) \ . \tag{33}$$

As a consequence, the original double integral has been replaced by a simple sum and the fitting procedure made much less cumbersome.

Appendix B: prediction of parameter biases resulting from use of wrong constant values of some of them

Let $\mathbf{p}_0$ (assumed to be $\mathbf{0}$ for simplicity in this appendix) be the true value of the parameter vector, $\mathbf{p}_1$ and $\mathbf{p}_2$ the fit and non-fit parts of the parameter vector ($\mathbf{p}_2 = (\tau)$ or $(f_v, \tau)^T$), and ϵ_2 be the error in $\mathbf{p}_2$. Fitting only $\mathbf{p}_1$ will provide a biased estimate $\hat{\mathbf{p}}$:

$$\hat{\mathbf{p}} = \mathbf{p}_0 + (\mathbf{b}_1, \epsilon_2)^T . \tag{34}$$

The problem is to estimate the bias $\mathbf{b}_1$ in the fit parameters due to the error ϵ_2 in the non-fit parameters. Assuming that a second order expansion of the χ^2 criterion in $\hat{\mathbf{p}}$ is valid:

$$\chi^2(\hat{\mathbf{p}}) = \chi^2(\mathbf{p}_0) + \mathbf{p}^T M \ \mathbf{p} \tag{35}$$

where the matrix M is defined as:

$$M = \left(\frac{\partial y(\mathbf{p})}{\partial \mathbf{p}}\right)^T_{|\mathbf{p}_0} \Sigma^{-1} \left(\frac{\partial y(\mathbf{p})}{\partial \mathbf{p}}\right)_{|\mathbf{p}_0} = \begin{pmatrix} M_{11} & M_{12} \\ M_{21} & M_{22} \end{pmatrix} \tag{36}$$

then with $\mathbf{p} = (\mathbf{p}_1, \mathbf{p}_2)^T$, χ^2 can be written:

$$\chi^2 = \mathbf{p}_1^T M_{11} \ \mathbf{p}_1 + (\mathbf{p}_1^T M_{12} \ \mathbf{p}_2 + \mathbf{p}_2^T M_{21} \ \mathbf{p}_1) + \mathbf{p}_2^T M_{22} \ \mathbf{p}_2 \tag{37}$$

the new optimum $\hat{\mathbf{p}}$ is defined by:

$$\frac{\partial \chi^2}{\partial \mathbf{p}_{1\,|\hat{\mathbf{p}}}} = \mathbf{0} , \tag{38}$$

and therefore:

$$M_{11} \ \mathbf{b}_1 + M_{12} \ \epsilon_2 = \mathbf{0} \tag{39}$$

and:

$$\mathbf{b}_1 = -M_{11}^{-1} M_{12} \ \epsilon_2 . \tag{40}$$

Notice the linearity between the bias $\mathbf{b}_1$ in the fit parameters and the error ϵ_2 in the non-fit parameters.

Acknowledgements

This work was supported in part by the Director, Office of Energy Research, Office of Health and Environmental Research of the US Department of Energy under contract No DE-AC03-76SF00098 and in part by Public Health Service Grant No HL25840 awarded by the National Heart Lung and Blood Institute, Department of Health and Human Services. Bernard Mazoyer acknowledges the support of part of this research by the Institut National de la Recherche en Informatique et Automatique (INRIA) and the Fondation pour la Recherche Médicale during 1984.

REFERENCES

1. BUDINGER TF, HUESMAN RH, KNITTEL B, FRIEDLAND R, DERENZO SE. Physiological modeling of dynamic measurements of metabolism using positron emission tomography. In: Greitz T et al. eds. *The metabolism of the human brain studied with positron emission tomography.* New York: Raven Press, 1985:165-183.

2. BECK JV, ARNOLD KJ, eds. *Parameter estimation in engineering and science.* New York: Wiley, 1977.

3. HUESMAN RH. A new fast algorithm for the evaluation of regions of interest and statistical uncertainty in computed tomography. *Phys Med Biol* 1984;29:543-552.

4. SOKOLOFF L, REIVICH M, KENNEDY C, et al. The (14C) deoxyglucose method for the measurement of local cerebral glucose utilization: Theory, procedure and normal values in the conscious and anesthetized albino rat. *J Neurochem* 1977;28:897-916.

5. PHELPS ME, HUANG SC, HOFFMAN EJ, SELIN C, SOKOLOFF L, KUHL DE. Tomographic measurement of local cerebral glucose metabolic rate in humans with (F-18)2-Fluoro-2-Deoxy-d-Glucose: Validation of the method. *Ann Neurol* 1979;6:371-388.

6. PARKER JA, BELLER GA, HOOP B, HOLMAN BL, SMITH TW. Assessment of regional myocardial blood flow and regional fractional oxygen extraction in dogs, using ^{15}O-Water and ^{15}O-Hemoglobin. *Circ Res* 1977;42:511-518.

7. SNYDER DL. Statistical analysis of dynamic tracer data. *IEEE Trans Biomed Eng* 1973;BME-20:11-20.

8. EYKOFF P ed. *System identification: Parameter and state estimation.* New York: Wiley, 1974.

9. EADIE WT, DRIJARD D, JAMES FE, ROOS M, SADOULET B. *Statistical methods in experimental physics.* Amsterdam: North-Holland, 1971.

10. FRIEDLAND RP, BUDINGER TF, GANZ E, et al. Regional cerebral metabolic alterations in dementia of the Alzheimer type: Positron emission tomography with [18F]Fluorodeoxyglucose. *J Comput Assist Tomogr* 1983;7:590-598.

11. KNITTEL B. Kinetic analysis of dynamic PET data. *Lawrence Berkeley Laboratory Report No 17313*, 1983.

12. MARQUARDT DW. An algorithm for least-squares estimation of nonlinear parameters. *SIAM* 1963;11:431-441.

13. MEHRA RK. Optimal input signals for parameter estimation in dynamic systems: Survey and new results. *IEEE Trans Autom Cont* 1974;AC-19:753-768.

14. DI STEFANO JJ III. Optimized blood sampling protocols and sequential design of kinetic experiments. *Am J Physiol* 1981;R259-265.

15. MORI F, DI STEFANO JJ III. Optimal nonuniform sampling interval and test-input design for identification of physiological systems from very limited data. *IEEE Trans Autom Cont* 1979;AC-24:893-900.

16. CRAMER H. *Mathematical methods of statistics.* Princeton: Princeton University Press, 1958.

This report was done with support from the Department of Energy. Any conclusions or opinions expressed in this report represent solely those of the author(s) and not necessarily those of The Regents of the University of California, the Lawrence Berkeley Laboratory or the Department of Energy.

Reference to a company or product name does not imply approval or recommendation of the product by the University of California or the U.S. Department of Energy to the exclusion of others that may be suitable.

TECHNICAL INFORMATION DEPARTMENT
LAWRENCE BERKELEY LABORATORY
UNIVERSITY OF CALIFORNIA
BERKELEY, CALIFORNIA 94720